Computers, Materials & Continua

Tech Science Press

DOI: 10.32604/cmc.2023.037514
*Article*

# Improved Transient Search Optimization with Machine Learning Based Behavior Recognition on Body Sensor Data

**Baraa Wasfi Salim[1], Bzar Khidir Hussan[2], Zainab Salih Ageed[3] and Subhi R. M. Zeebaree[4,*]**

[1]ITM Department, Technical College of Administration, Duhok Polytechnic University, Duhok, Iraq
[2]Information System Engineering Department, Erbil Technical Engineering College, Erbil Polytechnic University, Erbil, Iraq
[3]Computer Science Department, College of Science, Nawroz University, Duhok, Iraq
[4]Energy Eng. Department, Technical College of Engineering, Duhok Polytechnic University, Duhok, Iraq
*Corresponding Author: Subhi R. M. Zeebaree. Email: subhi.rafeeq@dpu.edu.krd
Received: 07 November 2022; Accepted: 08 February 2023

**Abstract:** Recently, human healthcare from body sensor data has gained considerable interest from a wide variety of human-computer communication and pattern analysis research owing to their real-time applications namely smart healthcare systems. Even though there are various forms of utilizing distributed sensors to monitor the behavior of people and vital signs, physical human action recognition (HAR) through body sensors gives useful information about the lifestyle and functionality of an individual. This article concentrates on the design of an Improved Transient Search Optimization with Machine Learning based Behavior Recognition (ITSOML-BR) technique using body sensor data. The presented ITSOML-BR technique collects data from different body sensors namely electrocardiography (ECG), accelerometer, and magnetometer. In addition, the ITSOML-BR technique extract features like variance, mean, skewness, and standard deviation. Moreover, the presented ITSOML-BR technique executes a micro neural network (MNN) which can be employed for long term healthcare monitoring and classification. Furthermore, the parameters related to the MNN model are optimally selected via the ITSO algorithm. The experimental result analysis of the ITSOML-BR technique is tested on the MHEALTH dataset. The comprehensive comparison study reported a higher result for the ITSOML-BR approach over other existing approaches with maximum accuracy of 99.60%.

**Keywords:** Behavior recognition; transient search optimization; machine learning; healthcare; sensors; wearables

## 1 Introduction

Recent advancements in sensing technologies have enabled the healthcare industry to enhance the quality of its services [1]. Additionally, the design of lightweight and small smart sensors has enabled

mechanisms to act as a vital part of advanced progress in unobtrusive and unsupervised methods of home rehabilitation and the continual monitoring of patient's health conditions. Nowadays, body sensors are becoming very popular for several realistic applications like healthcare, entertainment, security, and wellness [2]. One key benefit of utilizing body sensors in observing people is employed to recognize the behavior and vital signs of people very precisely than the ambient sensors. Thus, body sensors or personal computers were anticipated to take a disruptive effect on our life [3]. Therefore, the sensor will be implemented for ensuring and improving a person's sound living. Hence, the body sensor is quite striking to aid in transforming our life like a personal computer. During the commercial domains, a wearable sensor-related mechanism was utilized in the procedure of emergency buttons for asking for emergency aid, and it is commercially successful so far [4]. Recently, human activity recognition (HAR) in wearable body sensor network has gained popularity because of its immense effectiveness in various application regions like smart homes, smart healthcare, transportation, robotics, and security. HAR mechanism generally transforms particular body movements sensed by several wearable body sensors for certain sensor signal paradigms and is categorized through machine learning (ML) approaches [5]. For instance, many ML techniques were employed for identifying complicated activity paradigms like relaxing and sitting, climbing stairs, lying down, walking, and many more. Accordingly, recognition of day-to-day activities becomes essential for maintaining a healthy lifestyle between old people for preventing and monitoring serious illnesses [6].

But recognizing human activity becomes a challenge in the Internet of Medical Things (IoMT) field because of the current utility of batteryless or passive wearable body sensors for recognizing activity [7]. Such sensors will be lightweight and tiny, thus, are easily entrenched into patients' clothes for unobtrusive activity monitoring. Furthermore, it is easily preserved as it does not employ any battery. Such inactive wearable body sensors seize data through harvested power technologies that denote such sensors should receive energy to function and sense data [8]. Conventional ML approaches like support vector machine and hidden Markov models (HMM) could not be directly applied to detecting action in passive sensor data since they are concentrated on single sensing modalities that have a regular sampling rate of data [9]. Furthermore, such techniques encounter difficulty when the features count were less, therefore offering the outcomes with minimal accuracy. Currently, deep learning (DL) techniques were employed to recognize human action from body sensor information in the IoMT platform. DL was a kind of neural network (NNs) that uses several non-linear data processing layers to derive features and carry out classification [10].

This article concentrates on the design of an Improved Transient Search Optimization with Machine Learning based Behavior Recognition (ITSOML-BR) technique using body sensor data. The presented ITSOML-BR technique collects data from different body sensors namely magnetometer, electrocardiography (ECG), and accelerometer. In addition, the ITSOML-BR technique extract features like variance, mean, skewness, and standard deviation. Moreover, the presented ITSOML-BR technique executes micro neural network (MNN) which can be employed for long term healthcare monitoring and classification. Furthermore, the parameters related to the MNN model are optimally selected via the ITSO algorithm. The experimental result analysis of the ITSOML-BR technique is tested on the MHEALTH dataset.

The rest of the paper is organized as follows. Section 2 offers a brief related review of HAR models and Section 3 introduces the proposed model. Later, Section 4 provides experimental validation and Section 5 concludes the study.

## 2 Related Works

The author in [11] developed the generic HAR architecture for cell phone sensor data dependent upon long short term memory (LSTM) network for the time sequence domain. Four benchmark LSTM networks are relatively analyzed to study the effect of utilizing various cell phone sensor information. Furthermore, a hybrid LSTM network named 4-layer convolutional neural network (CNN)-LSTM is intended for improving detection accuracy. Wang et al. [12] developed a deep learning (DL) based system that finds the changes and certain actions amongst two dissimilar activities of lower frequency and shorter duration for healthcare applications. In the presented technique, a deep convolutional neural network (DCNN) is generated for extracting features from the information gathered by the sensor. Afterward, the LTSM network is utilized for capturing long-term dependency among 2 activities to moreover enhancing the HAR rate of detection. With the incorporation of LSTM and CNN, a wearable sensor based method is developed which specifically identifies transition and activity.

Nafea et al. [13] introduce a technique based on CNN with different kernel dimensional and bidirectional LSTM (Bi-LSTM) for capturing feature at different resolutions. The advance of this study lies in the efficiency selective of optimal video demonstration and in the efficient extraction of spatial and temporal characteristics in sensor information utilizing Bi-LSTM and CNN. Ghate [14] introduces different hybrid DL methodologies which integrate deep neural network (DNN) with other modules such as gated recurrent unit (GRU) and LSTM Models for efficient classification of engineered features from CNN. A modern framework which incorporates DCNN with random forest (RF) Classifiers for adding randomness to the model. The authors in [15] developed the transformer module, a DL-NN for the vision, and natural language processing (NLP) tasks are adopted for a time-sequence examination of motion signal.

A novel DNN framework for HAR dependent upon multiple sensor information was developed in [16]. Especially, the presented method encoder the time sequence of sensor information as images (encode one time series as to 2-channel image) and leverages the changed image to preserve the essential features of HAR. Especially, to permit heterogeneous sensor information that is cooperatively trained, the authors adopt fusion residual networks by combining 2 networks and training heterogeneous information with pixel-wise correspondence. Mondal et al. [17] introduced an end-to-end fast GNN that captures the individual sample data and the relationships with another instance in the procedure of undirected graph infrastructure. The time sequence information is converted into a structural demonstration of graph for HAR utilizing sensor information.

## 3 The Proposed Model

In this article, a novel ITSOML-BR system was introduced for the recognition of behaviors on-body sensor data. At the preliminary level, the presented ITSOML-BR technique performs the data collection phase using various body sensors, namely ECG, accelerometer, and magnetometer. Followed by the ITSOML-BR technique extracted the features, namely standard deviation, mean, skewness, and variance. For behavior recognition, the presented ITSOML-BR technique executed the MNN model for long-term healthcare monitoring and classification. Fig. 1 defines the overall process of the ITSOML-BR system.

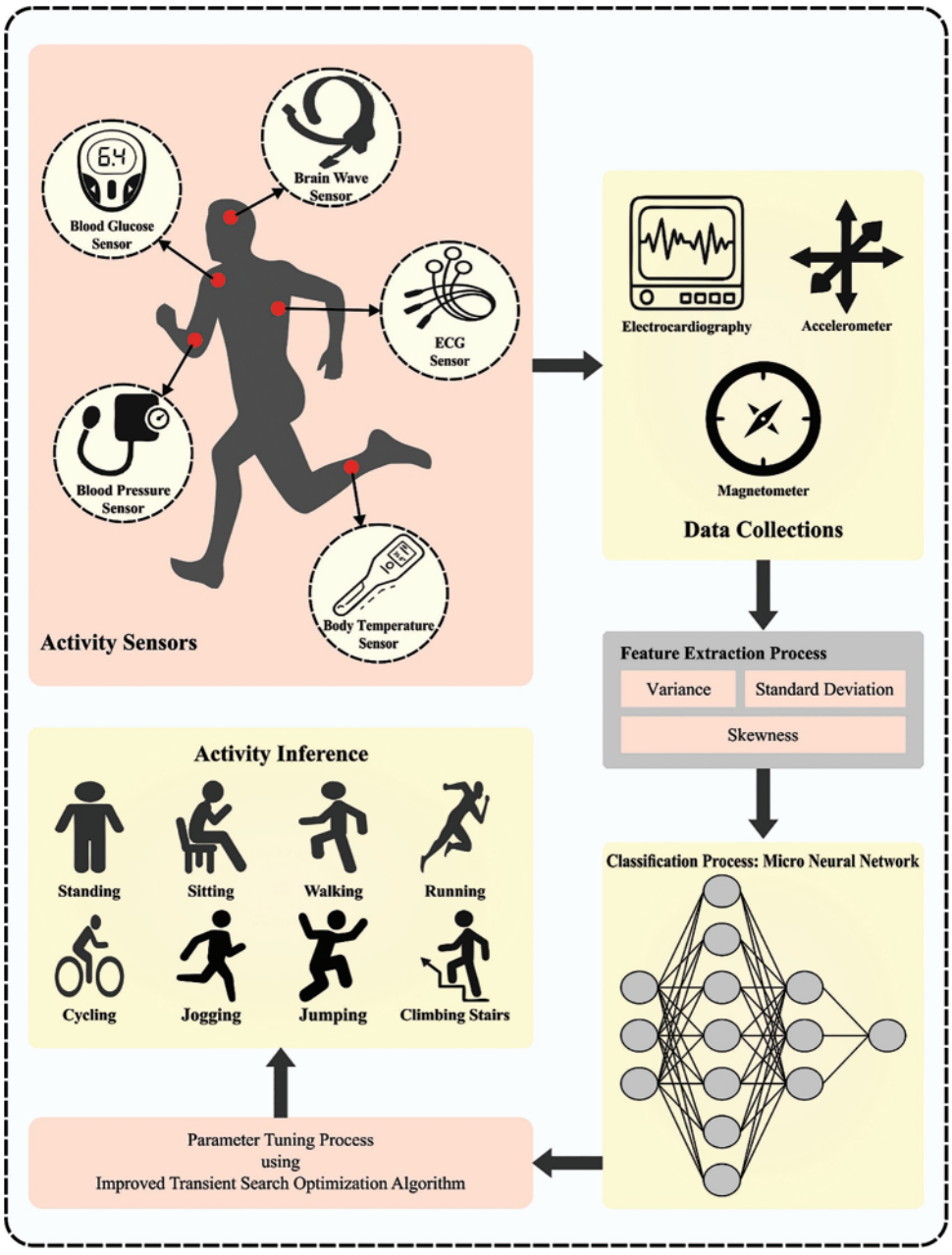


**Figure 1:** Overall process of ITSOML-BR system

### *3.1 Data Collection Module*

At the introductory level, the presented ITSOML-BR technique performs the data collection phase using various body sensors namely ECG, accelerometer, and magnetometer. The place of attaching sensor is the chest, left ankle, and right wrist [18]. There exists an ECG health care sensor positioned on the chest that takes 2-lead ECG measurements of heart information. For example, the

accelerometer provides magnetometer magnetic field orientation, body acceleration, and gyroscope the rate of turn. The body sensor information is characterized by the following.

$$C_C = (A_x,\ A_y,\ A_z). \tag{1}$$

ECG sensor information in the chest is given by

$$G = g_1 || g_2. \tag{2}$$

The accelerometer sensor information in the left ankle is shown below

$$C_{LA} = (L_x,\ L_y,\ L_z). \tag{3}$$

The gyroscope sensor information in the left ankle is symbolized by

$$Y_{LA} = (R_x,\ R_y,\ R_z). \tag{4}$$

The magnetometer sensor information in the left ankle is shown below

$$N_{LA} = (T_x,\ T_y,\ T_z). \tag{5}$$

The accelerometer sensor information in the right wrist is given by

$$A_{RW} = (I_x,\ I_y,\ I_z). \tag{6}$$

The gyroscope sensor information from the left wrist is characterized by

$$R_{LW} = (S_x,\ S_y,\ S_z). \tag{7}$$

The gyroscope sensor information from the right wrist is considered as

$$R_{RW} = (W_x,\ W_y,\ W_z). \tag{8}$$

The magnetometer information on the right wrist is given by

$$N_{RW} = (E_x,\ E_y,\ E_z). \tag{9}$$

Moreover, features like mean $m$, variance $v$, standard deviation $s$, and skewness $w$ are extracted from the information. Next, the feature attained in a signal of a certain period for the activity are combined by increasing them horizontally as $F$.

### *3.2 Behavior Recognition Module*

For behavior recognition, the presented ITSOML-BR technique executed the MNN model. Assume that the recurrent neural network (RNN) has a memory function while processing medicinal time sequence data and that its volume is small compared to the CNN [19]. Based on the shallow RNN, this study primarily adopted the set of multi-level RNNs as the feature extractor.

Initially, it can be set RNN gathered with 2 levels. Then, the slice data is set afterwards pre-processing as $S_i = \{v_1,\ v_2,\ \ldots,\ v_r\}$, and split into slices that size is $\omega$. $S_i$ generates $n/\omega$ slices, and we utilized $A_k$ to represent all the slices in the following:

$$\beta_k^{[1]} = RNN^{[1]}(A_k),\ k \in \left[1, \frac{n}{\omega}\right]. \tag{10}$$

Now, RNN characterizes the RNN technique of the initial level, and $\beta_k^{[1]}$ indicates the outcome of the $k^{th}$ slice by RNN. Thus, we obtain the outcome $\left[\beta_1^{[1]}, \beta_2^{[1]}, \ldots, \beta_{n/\omega}^{[1]}\right]$ afterward training of RNN collection of the initial level.

Next, the outcome is fed to the RNN of the second level, and the outcome can be denoted as follows:

$$\beta^{[2]} = RNN^{[2]}\left(\beta_1^{[1]}, \beta_2^{[1]}, \ldots, \beta_{\frac{n}{\omega}}^{[1]}\right), = \mathrm{F}\left(\beta^{[2]}\right), \tag{11}$$

Whereas RNN signifies the RNN model of the next level, $F$ denotes the activation function, and $y$ represents the extracted feature. During the selective technique for MicroNN, a per-class classifier algorithm is adopted. $e$ module establishes a separate mini-classifier for all the classes. Each mini-classifier is interconnected with the feature extractor. Furthermore, to enhance the classifier efficiency, a loss function is employed named one-class:

$$loss = E_{X\sim P_X^{class_i}}\left[-\log\ \left(\sigma\left(f_i\left(X\right)\right)\right)\right] + \eta \cdot E_{X\sim P_X^{class_i}}\left\|\frac{\partial f_i\left(X\right)}{\partial X}\right\|_2^c + \pi \cdot \left\|\theta_i - \mu_{1:i-1}^*\right\|_2^2, \tag{12}$$

where $X \sim P_X^{class_i}$ denotes all classes' data distribution, $\sigma$ shows the activation function, $\eta$, $c$, and $\pi$ indicate each hyperparameter. The initial term in the loss function has a negative log probability. It aims to maximize the score of $class_i$ in the trained. But if there exists no limitation to the negative log probability, it leads to an unconstrained increment in the score. The architecture of the per-class classifier is the multilayer perceptron (MLP) with 3 layers, as given below.

$$E_{X\sim P_X^{class_i}}\left\|\frac{\partial f_i\left(X\right)}{\partial X}\right\|_2^c = E_{X\sim P_X^{class_i}}\left\|\frac{\partial W_3 \cdot \left[\sigma\left(W_2 \cdot \sigma\left(W_1 \cdot X\right)\right)\right]}{\partial X}\right\|_2^c \tag{13}$$

Note that the derivative outcome of $H$-reg in the training procedure is associated with the weight ($W_1$, $W_2$ *and* $W_3$).

Consequently, $H$-reg restricts the phenomenon of the unrestrained increase of weighted that the negative log probability brings.

For making the parameter of classifiers among distinct classes in a similar variable space, the technique uses the parameter from 1 to $i-1$ mini-classifier for initializing the parameter of $i^{th}$ mini-classifier. Considering the presence of similar features among distinct classes, the DL model has complex differentiating classes during training. In the testing phase, a technique based on $KL$-divergence is utilized for reducing shared knowledge among the classes, as defined in the third term of loss functions. Assume that a $T$ mini-classifier exists in MicroNN, the computation of shared knowledge amongst $T$ mini-classifiers.

$$\rho_{1:T}^* = \ \mathrm{argmin} \sum_{i=1}^{T} \phi_i KL\ \left(P_i \| P_{1:T}\right), \tag{14}$$

$\phi_i$ denotes the mixing ratio with $\sum_{i=1}^{T}\phi_i = 1$, and $P_i$ signifies the posterior variable distribution of $i^{th}$ mini-classifiers. $e$ parameter of $i^{th}$ mini classifiers are upgraded as follows.

$$\theta_i^* = \theta_i - \tau \cdot \rho_{1:T}^*, \tag{15}$$

whereas $\tau$ denotes the hyperparameter.

### *3.3 Parameter Adjustment Module*

In this work, the parameters related to the MNN model are optimally selected via the ITSO algorithm. The TSOA is an alternative model based on electrical phenomena that incorporate two energy-saving mechanisms [20]. This can be inspired by the transient response (TR) of a switched electrical circuit (SEC). This component is a capacitor, resistor, and inductor. Therefore, the response-based voltage based on the capacitor in the circuit of R-C and R-L-C can be determined in the following:

$$v_1(t) = v_1(\infty) + (v_1(0) - v_1(\infty))\, e^{\frac{-t}{R_1 C_1}} \tag{16}$$

$$v_2(t) = e^{\frac{-R_2 t}{2L}} (\beta_1 \cos(2\pi f_d t) + \beta_2 \sin(2\pi f_d t)) + v_2(\infty);\ if\ \left(\frac{R_2}{2L}\right)^2 < \frac{1}{LC_2} \tag{17}$$

$R$, $L$, and $C$ represent resistance, inductor and capacitors; correspondingly, $v_1(t)$ and $v_2(t)$ denote the response of R-C and R-L-C circuits. Also, $f_d$ indicates the damping frequency, and $Bl$ and $B2$ indicate the constant number. Hence, the voltage response of the abovementioned circuit in Eqs. (16) and (17) are employed to model the TSOA. In this work, $R$, $L$, and $C(R1, R2, C1, C2$ and $L)$ in $V(t)$ and $v(t)$ are transformed into arbitrary numbers as $U$ and $\alpha$. These random characteristics are desired for the optimized method.

The decision variable in TSOA is regarded as searching agent $X_{IT}+1$ and $X_{IT}$, that is corresponding to $v(t)$ and $v(0)$ parameters. Similarly, the $X^{ba}$ represents the parameter presented as the better agent and corresponds to $(\infty)$. Furthermore, in the equation of $v_2(t)$, $\beta_1 = \beta_2 = \left|X_{IT} - WX^{ba}_{IT*}\right|$ is determined whereby $U$ random integer is determined as $U = k \times rm_2 \times a + 1$ that $k$ represents the actual number and $rm_2$ shows the random number within [0, 1]. The $r_1$ is employed to balance the exploration and exploitation stages with $rm_1 \geq 0.5$ and $rm_1 < 0.5$, correspondingly in the TSOA.

$$X_{IT+1} = \begin{cases} X^{*ba}_{IT} + \left(X_{IT} - U \times X^{*ba}_{IT}\right) e^{-\alpha}; & rm_1 < 0.5 \\ X^{*ba}_{IT} + e^{-\alpha} [\cos\ (2\pi\alpha) + \sin\ (2\pi\alpha)] \left|X_{IT} - U \times X^{*ba}_{IT}\right|; & rm_1 \geq 0.5 \end{cases} \tag{18}$$

$\mathrm{A} = 2 \times a \times rm_3 - a$, and $rm_3$ represent the real random number amongst [0, 1].

In the presented ITSO method, the *OLS* is employed to improve the balance of the exploitation and exploration and convergence efficiency of the TSOA. This algorithm might be trapped in local optima. This method is also time-consuming because of the variance between the optimal and initial solutions. Although this algorithm reaches the global optima, it may not have a better accuracy and convergence speed. Subsequently, the convergence speed rises. Assume $X$ is in $[\eta,\ \lambda]$. Then, the opposite points are $\bar{X} = \eta + \lambda - X.X = (X_1,\ X_2,\ \ldots,\ \mathrm{Xd})$, refer to a point in the searching region with $d$ dimension, whereas $X_1,\ X_2, \ldots,\ X_d \in R$ and $X_j \in [\eta_i,\ \lambda_j]; \forall i \in \{1, 2, \ldots, d\}$. The opposite point dependent upon the component is given below:

$$\overline{X} = \eta_i + \lambda_i - X_i, \overline{X} = \left(\overline{X}, \overline{X}, \ldots, \overline{X}\right) \tag{19}$$

Hence, the early population can be produced utilizing OLS.

The non-linearly decreasing strategy (NDS) is also employed for improving the TSOA efficiency in global and local explorations and accomplishing the desired balance between convergent efficiency and global convergence. Search efficiency is enhanced by the variations in the coefficient of $\partial^N s$. $\mathbb{E}e\partial^{NDS}$ non-linearly reduced from $\partial^{NDS}_{\max}$ to $\partial^{NDS}_{\min}$. The greater value of $\partial^{NDS}$ assists the best global search ability.

In addition, the small $\partial^{NDS}$ improves global search ability in the exploration stage.

$$\partial^{NSD} = \partial^{NDS}_{\max} - \frac{IT \times \left(\partial^{NDS}_{\max} - \partial^{NDS}_{\min}\right)}{IT^{\max}} \times \sin\left(\frac{IT \times \pi}{2 \times IT^{\max}}\right) \tag{20}$$

whereas, $\partial^{NDS}_{\max}$ and $\partial^{NDS}_{\min}$ represent the upper and lower limits of coefficient $\partial^{NDS}$, correspondingly

Hence Eq. (20) can be modified by

$$X_{IT+1} = \begin{cases} \partial^{NSD} X^{*ba}_{IT} + \left(X_{IT} - UX^{*ba}_{IT}\right) e^{-\alpha}; & rm_1 < 0.5 \\ \partial^{NSD} X^{*ba}_{IT} + \left|X_{IT} - UX^{*ba}_{IT}\right| e^{-\alpha} (\cos\ (2\pi\alpha) + \sin\ (2\pi\alpha)); & rm_1 \geq 0.5 \end{cases} \tag{21}$$

The ITSOA could have a higher global search ability in pre-search, and its convergence speed can be faster. Fig. 2 demonstrates the flowchart of ITSOA.

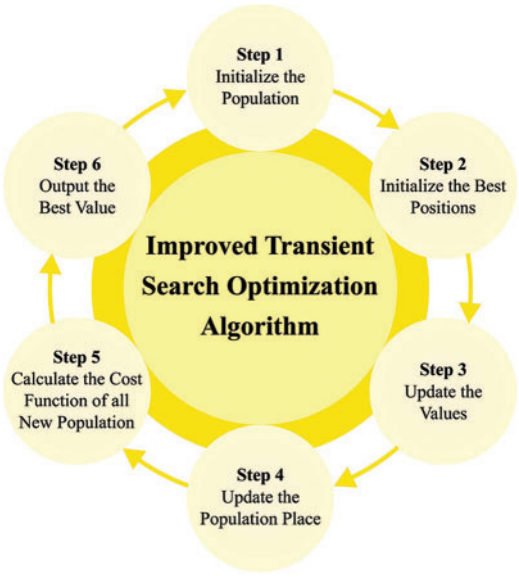


**Figure 2:** Flowchart of ITSO technique

The ITSO approach derives a fitness function from having better classification accuracy. It describes a positive integer to characterize the improved performance of the candidate solutions. During this study, the minimization of the classification error rate can be treated as the fitness function, as shown below.

$$\begin{aligned} fitness\,(x_i) &= Classifier\ Error\ Rate\,(x_i) \\ &= \frac{number\ of\ misclassified\ samples}{Total\ number\ of\ samples} * 100 \end{aligned} \tag{22}$$

## 4 Results and Discussion

The proposed model is simulated using Python 3.6.5 tool. The proposed model is experimented on PC i5-8600k, GeForce 1050Ti 4 GB, 16 GB RAM, 250 GB SSD, and 1 TB HDD. The parameter settings are given as follows: learning rate: 0.01, dropout: 0.5, batch size: 5, epoch count: 50, and activation: ReLU.

In this section, the behavior recognition of the ITSOML-BR approach is tested using the MHEALTH database [21], which is gathered from a set of 10 persons by the use of body motion and vital sign recordings of the SHIMMER2 wearable sensor. Table 1 defines the detailed description of the dataset.

**Table 1:** Details of the dataset

| Label | Classes | Repetitions/durations | No. of samples |
|---|---|---|---|
| L1 | Standing still | 1 min | 1000 |
| L2 | Sitting and relaxing | 1 min | 1000 |
| L3 | Lying down | 1 min | 1000 |
| L4 | Walking | 1 min | 1000 |
| LS | Climbing stairs | 1 min | 1000 |
| L6 | Waist bends forward | 20× | 1000 |
| L7 | Frontal elevation of arms | 20× | 1000 |
| L8 | Knees bending (crouching) | 20× | 1000 |
| L9 | Cycling | 1 min | 1000 |
| LI0 | Jogging | 1 min | 1000 |
| L11 | Running | 1 min | 1000 |
| L12 | Jump front & back | 20× | 1000 |
| **Total number of instances** | | | **12000** |

The confusion matrices of the ITSOML-BR model are examined under several sizes of training (TR) and testing (TS) database, as shown in Fig. 3. The presented ITSOML-BR model has effectually categorized the data under 12 class labels.

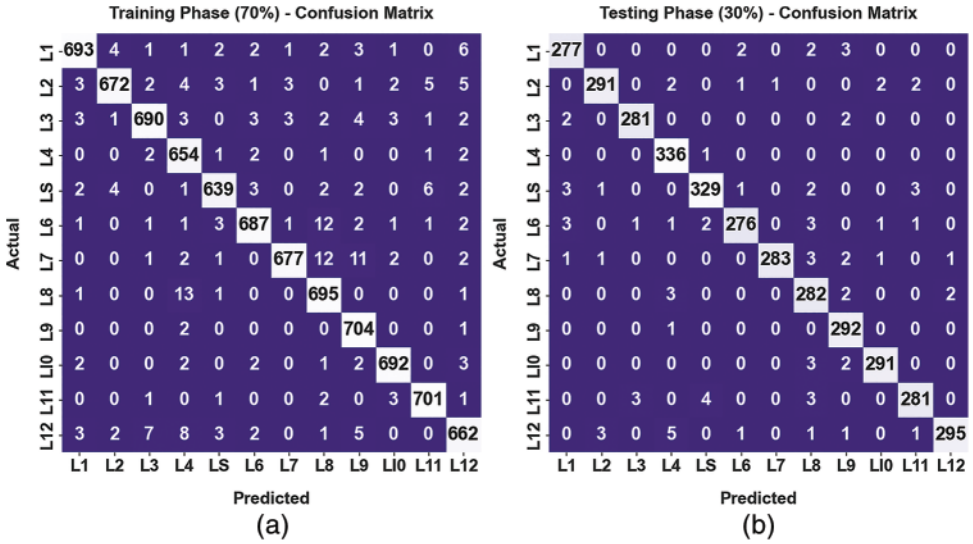


**Figure 3:** (Continued)

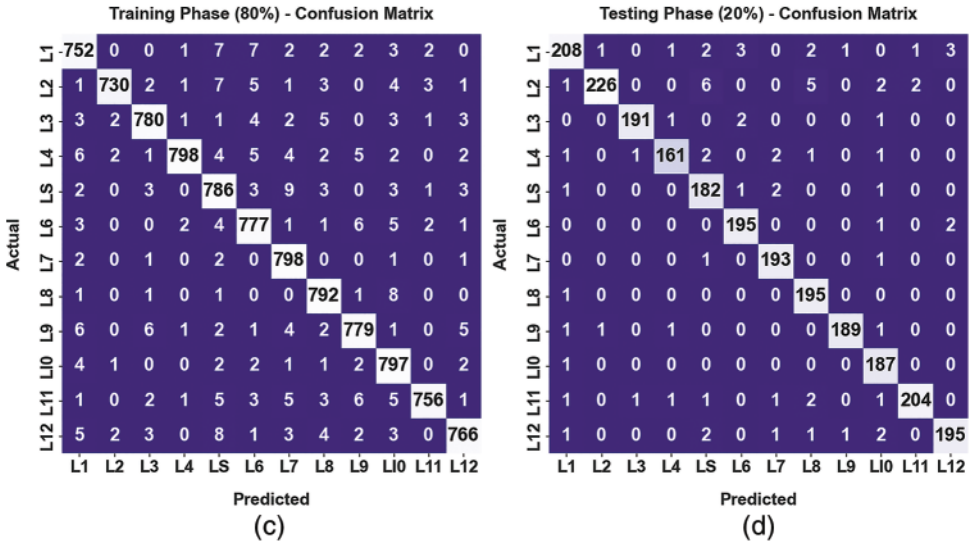


**Figure 3:** Confusion matrices of ITSOML-BR system (a–b) TR and TS database of 70:30 and (c–d) TR and TS database of 80:20

Table 2 and Fig. 4 exhibit an overall recognition performance of the ITSOML-BR model on 70% of the TR database. The simulation outcomes indicated that the ITSOML-BR approach has achieved effectual recognition under all class labels. The results inferred that the ITSOML-BR model has gained an average $accu_y$ of 99.54%, $sens_y$ of 97.22%, $spec_y$ of 99.75%, $F_{score}$ of 97.21%, and Mathew Correlation Coefficient (MCC) of 96.96%.

**Table 2:** Result analysis of ITSOML-BR system with varying class labels under 70% of the TR database

| Training phase (70%) | | | | | |
|---|---|---|---|---|---|
| Labels | $Accu_y$ | $Sens_y$ | $Spec_y$ | $F_{score}$ | MCC |
| L1 | 99.55 | 96.79 | 99.80 | 97.33 | 97.09 |
| L2 | 99.52 | 95.86 | 99.86 | 97.11 | 96.86 |
| L3 | 99.52 | 96.50 | 99.80 | 97.18 | 96.93 |
| L4 | 99.45 | 98.64 | 99.52 | 96.60 | 96.33 |
| LS | 99.56 | 96.67 | 99.81 | 97.19 | 96.95 |
| L6 | 99.52 | 96.49 | 99.80 | 97.17 | 96.91 |
| L7 | 99.54 | 95.62 | 99.90 | 97.20 | 96.96 |
| L8 | 99.39 | 97.75 | 99.54 | 96.46 | 96.14 |
| L9 | 99.61 | 99.58 | 99.61 | 97.71 | 97.52 |
| LI0 | 99.71 | 98.30 | 99.84 | 98.30 | 98.14 |
| L11 | 99.74 | 98.87 | 99.82 | 98.46 | 98.31 |
| L12 | 99.31 | 95.53 | 99.65 | 95.80 | 95.43 |
| **Average** | **99.54** | **97.22** | **99.75** | **97.21** | **96.96** |

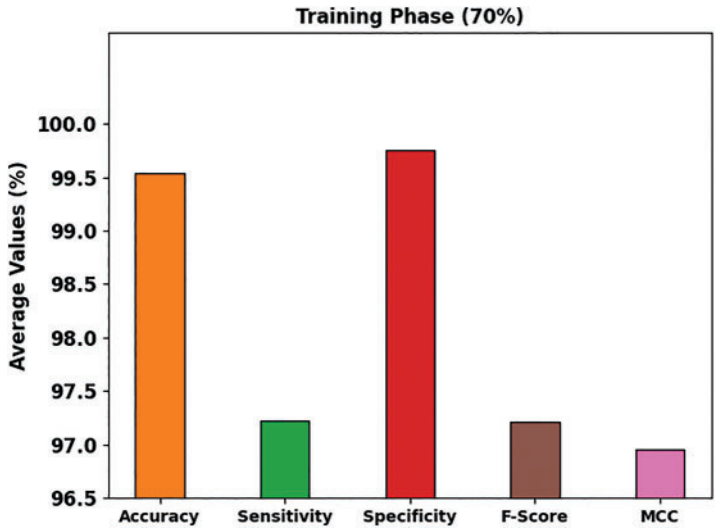


**Figure 4:** Average analysis of ITSOML-BR system under 70% of TR database

Table 3 and Fig. 5 demonstrate an overall recognition performance of the ITSOML-BR method on 30% of the TS database. The figure indicates that the ITSOML-BR system has achieved effectual recognition outcomes in all class labels. The outcomes revealed that the ITSOML-BR approach has attained an average $accu_y$ of 99.60%, $sens_y$ of 97.60%, $spec_y$ of 99.78%, $F_{score}$ of 97.61%, and MCC of 97.40%.

**Table 3:** Result analysis of ITSOML-BR system with varying class labels on 30% of the TS database

| Testing phase (30%) | | | | | |
|---|---|---|---|---|---|
| Labels | $Accu_y$ | $Sens_y$ | $Spec_y$ | $F_{score}$ | MCC |
| L1 | 99.56 | 97.54 | 99.73 | 97.19 | 96.95 |
| L2 | 99.64 | 97.32 | 99.85 | 97.82 | 97.62 |
| L3 | 99.78 | 98.60 | 99.88 | 98.60 | 98.48 |
| L4 | 99.64 | 99.70 | 99.63 | 98.10 | 97.92 |
| LS | 99.53 | 97.05 | 99.79 | 97.48 | 97.22 |
| L6 | 99.53 | 95.83 | 99.85 | 97.01 | 96.76 |
| L7 | 99.72 | 96.92 | 99.97 | 98.26 | 98.12 |
| L8 | 99.33 | 97.58 | 99.49 | 95.92 | 95.57 |
| L9 | 99.64 | 99.66 | 99.64 | 97.82 | 97.65 |
| LI0 | 99.75 | 98.31 | 99.88 | 98.48 | 98.34 |
| L11 | 99.53 | 96.56 | 99.79 | 97.06 | 96.81 |
| L12 | 99.58 | 96.09 | 99.91 | 97.52 | 97.31 |
| **Average** | **99.60** | **97.60** | **99.78** | **97.61** | **97.40** |

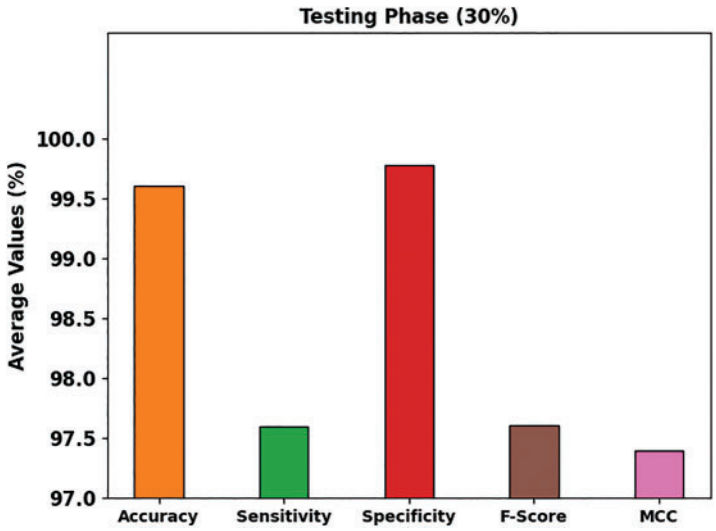


**Figure 5:** Average analysis of ITSOML-BR system under 30% of TS database

Table 4 and Fig. 6 showcase an overall recognition performance of the ITSOML-BR approach on 80% of the TR database. The simulation outcomes referred that the ITSOML-BR methodology has obtained effectual recognition results under all class labels. The results stated that the ITSOML-BR system had achieved an average $accu_y$ of 99.50%, $sens_y$ of 96.98%, $spec_y$ of 99.73%, $F_{score}$ of 96.99%, and MCC of 96.73%.

**Table 4:** Result analysis of ITSOML-BR system with varying class labels on 80% of the TR database

| Training phase (80%) | | | | | |
|---|---|---|---|---|---|
| Labels | $Accu_y$ | $Sens_y$ | $Spec_y$ | $F_{score}$ | MCC |
| L1 | 99.38 | 96.66 | 99.61 | 96.16 | 95.82 |
| L2 | 99.64 | 96.31 | 99.92 | 97.66 | 97.47 |
| L3 | 99.54 | 96.89 | 99.78 | 97.26 | 97.01 |
| L4 | 99.58 | 96.03 | 99.92 | 97.56 | 97.34 |
| LS | 99.27 | 96.68 | 99.51 | 95.74 | 95.34 |
| L6 | 99.42 | 96.88 | 99.65 | 96.52 | 96.20 |
| L7 | 99.59 | 99.13 | 99.64 | 97.61 | 97.41 |
| L8 | 99.60 | 98.51 | 99.70 | 97.66 | 97.45 |
| L9 | 99.46 | 96.53 | 99.73 | 96.77 | 96.47 |
| LI0 | 99.45 | 98.15 | 99.57 | 96.78 | 96.49 |
| L11 | 99.57 | 95.94 | 99.90 | 97.36 | 97.14 |
| L12 | 99.48 | 96.11 | 99.78 | 96.84 | 96.56 |
| **Average** | **99.50** | **96.98** | **99.73** | **96.99** | **96.73** |

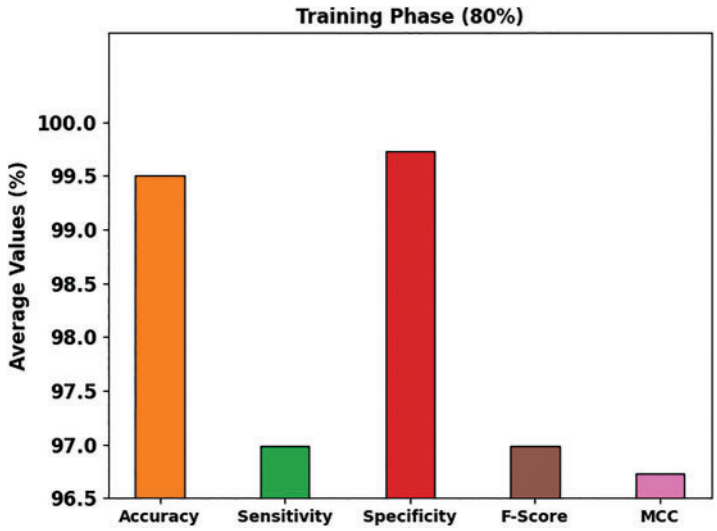


**Figure 6:** Average analysis of ITSOML-BR system on 80% of TR database

Table 5 and Fig. 7 depict an overall recognition performance of the ITSOML-BR algorithm on 20% of the TS database. The simulation outcomes revealed that the ITSOML-BR approach has achieved effective recognition under all class labels. The outcomes indicated that the ITSOML-BR technique has reached an average $accu_y$ of 99.49%, $sens_y$ of 97.02%, $spec_y$ of 99.72%, $F_{score}$ of 96.94%, and MCC of 96.67%.

**Table 5:** Result analysis of ITSOML-BR system with varying class labels under 20% of the TS database

| Testing phase (20%) | | | | | |
|---|---|---|---|---|---|
| Labels | $Accu_y$ | $Sens_y$ | $Spec_y$ | $F_{score}$ | MCC |
| L1 | 99.08 | 93.69 | 99.63 | 94.98 | 94.48 |
| L2 | 99.25 | 93.39 | 99.91 | 96.17 | 95.81 |
| L3 | 99.75 | 97.95 | 99.91 | 98.45 | 98.32 |
| L4 | 99.50 | 95.27 | 99.82 | 96.41 | 96.15 |
| LS | 99.21 | 97.33 | 99.37 | 95.04 | 94.64 |
| L6 | 99.62 | 98.48 | 99.73 | 97.74 | 97.54 |
| L7 | 99.67 | 98.97 | 99.73 | 97.97 | 97.79 |
| L8 | 99.50 | 99.49 | 99.50 | 97.01 | 96.78 |
| L9 | 99.75 | 97.93 | 99.91 | 98.44 | 98.30 |
| LI0 | 99.50 | 99.47 | 99.50 | 96.89 | 96.66 |
| L11 | 99.54 | 96.23 | 99.86 | 97.37 | 97.13 |
| L12 | 99.46 | 96.06 | 99.77 | 96.77 | 96.48 |
| **Average** | **99.49** | **97.02** | **99.72** | **96.94** | **96.67** |

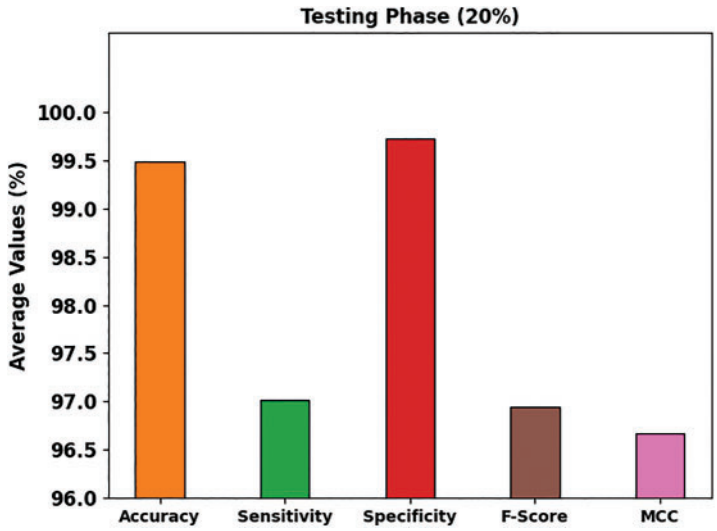


**Figure 7:** Average analysis of ITSOML-BR system under 20% of TS database

The training accuracy ($TR_{acc}$) and validation accuracy ($VL_{acc}$) gained by the ITSOML-BR algorithm under the test database is exposed in Fig. 8. The simulation result pointed out the ITSOML-BR algorithm has gained increased values of $TR_{acc}$ and $VL_{acc}$. In certain, the $VL_{acc}$ looked that better than $TR_{acc}$.

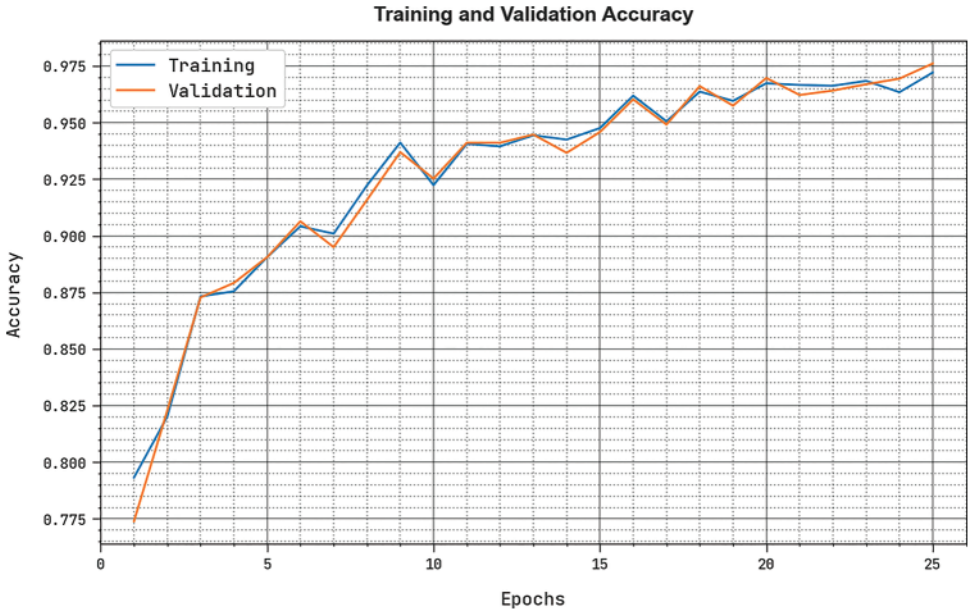


**Figure 8:** $TR_{acc}$ and $VL_{acc}$ analysis of ITSOML-BR system

The training loss ($TR_{loss}$) and validation loss ($VL_{loss}$) realized by the ITSOML-BR system under test database are exhibited in Fig. 9. The simulation result represented that the ITSOML-BR approach has obtained lower values of $TR_{loss}$ and $VL_{loss}$. In particular, the $VL_{loss}$ is lesser than $TR_{loss}$.


**Figure 9:** $TR_{loss}$ and $VL_{loss}$ analysis of ITSOML-BR system

To depict the improved performance of the ITSOML-BR approach, a detailed comparison study is made in Table 6 and Fig. 10. The simulation values indicated that the ITSOML-BR method has shown enhanced performance over other models with a maximum $accu_y$ of 99.60%.

At the same time, the Deep simple recurrent unit (SRU) approach has demonstrated lower classification performance. Although the other existing techniques have attained closer performance, the ITSOML-BR model has reached maximum classification performance.

**Table 6:** Comparative analysis of ITSOML-BR system with other algorithms

| Methods | Accuracy | Sensitivity | Specificity | F-Score |
|---|---|---|---|---|
| ITSOML-BR | 99.60 | 97.60 | 99.78 | 97.61 |
| Deep SRU | 94.20 | 96.50 | 98.13 | 96.46 |
| Deep SRU-GRU | 99.32 | 96.34 | 98.70 | 96.52 |
| ELM | 98.17 | 96.53 | 98.13 | 96.03 |
| KELM | 96.04 | 96.11 | 96.60 | 96.36 |
| DNN | 96.01 | 96.59 | 96.11 | 95.85 |

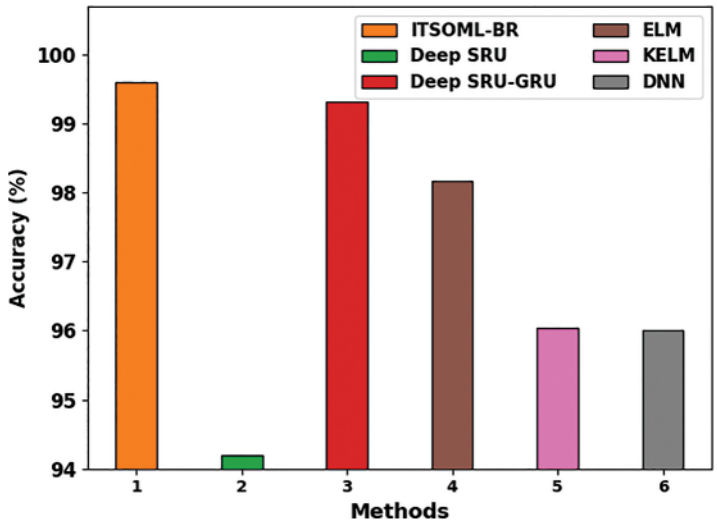


**Figure 10:** Comparative analysis of ITSOML-BR system with other approaches

## 5 Conclusion

This article introduced a novel ITSOML-BR system to recognise behaviors on-body sensor data. At the preliminary level, the presented ITSOML-BR technique performs the data collection phase using various body sensors, namely ECG, accelerometer, and magnetometer. Followed by the ITSOML-BR technique extracted the features like variance, mean, skewness, and standard deviation. For behavior recognition, the presented ITSOML-BR technique executed the MNN model for long-term healthcare monitoring and classification. At last, the parameters related to the MNN model are optimally selected via the ITSO algorithm. The experimental result analysis of the ITSOML-BR technique is tested on the MHEALTH dataset. The comprehensive comparison study reported the improved outcome of the ITSOML-BR methodology over other existing approaches with maximum accuracy of 99.60%. In future, the performance of the proposed model can be improved by hybrid DL classifiers.

**Funding Statement:** The authors received no specific funding for this study.

**Conflicts of Interest:** The authors declare that they have no conflicts of interest to report regarding the present study.

## References

[1] K. Chen, D. Zhang, L. Yao, B. Guo, Z. Yu *et al.,* "Deep learning for sensor-based human activity recognition: Overview, challenges, and opportunities," *ACM Computing Surveys (CSUR)*, vol. 54, no. 4, pp. 1–40, 2021.

[2] L. M. Dang, K. Min, H. Wang, M. J. Piran, C. H. Lee *et al.,* "Sensor-based and vision-based human activity recognition: A comprehensive survey," *Pattern Recognition*, vol. 108, pp. 107561, 2020.

[3] W. Gao, L. Zhang, W. Huang, F. Min, J. He *et al.,* "Deep neural networks for sensor-based human activity recognition using selective kernel convolution," *IEEE Transactions on Instrumentation and Measurement*, vol. 70, pp. 1–13, 2021.

[4] F. E. Erukainure, V. Parque, M. A. Hassan and A. M. R. FathEl-Bab, "Estimating the stiffness of kiwifruit based on the fusion of instantaneous tactile sensor data and machine learning schemes," *Computers and Electronics in Agriculture*, vol. 201, 2022. https://doi.org/10.1016/j.compag.2022.107289
[5] F. E. Erukainure, V. Parque, M. A. Hassan and A. M. R. FathElbab, "Towards estimating the stiffness of soft fruits using a piezoresistive tactile sensor and neural network schemes," in *2022 IEEE/ASME Int. Conf. on Advanced Intelligent Mechatronics (AIM)*, Hokkaido, Japan, pp. 290–295, 2022.
[6] N. Dua, S. N. Singh and V. B. Semwal, "Multi-input CNN-GRU based human activity recognition using wearable sensors," *Computing*, vol. 103, no. 7, pp. 1461–1478, 2021.
[7] J. Wang, Y. Chen, Y. Gu, Y. Xiao and H. Pan, "SensoryGANs: An effective generative adversarial framework for sensor-based human activity recognition," in *Int. Joint Conf. on Neural Networks (IJCNN)*, Rio de Janeiro, Brazil, pp. 1–8, 2018.
[8] S. Gupta, "Deep learning based human activity recognition (HAR) using wearable sensor data," *International Journal of Information Management Data Insights*, vol. 1, no. 2, pp. 100046, 2021.
[9] Q. Teng, K. Wang, L. Zhang and J. He, "The layer-wise training convolutional neural networks using local loss for sensor-based human activity recognition," *IEEE Sensors Journal*, vol. 20, no. 13, pp. 7265–7274, 2020.
[10] N. A. Choudhury, S. Moulik and D. S. Roy, "Physique-based human activity recognition using ensemble learning and smartphone sensors," *IEEE Sensors Journal*, vol. 21, no. 15, pp. 16852–16860, 2021.
[11] S. Mekruksavanich and A. Jitpattanakul, "Lstm networks using smartphone data for sensor-based human activity recognition in smart homes," *Sensors*, vol. 21, no. 5, pp. 1636, 2021.
[12] H. Wang, J. Zhao, J. Li, L. Tian, P. Tu *et al.,* "Wearable sensor-based human activity recognition using hybrid deep learning techniques," *Security and Communication Networks*, vol. 2020, pp. 1–12, 2020.
[13] O. Nafea, W. Abdul, G. Muhammad and M. Alsulaiman, "Sensor-based human activity recognition with spatio-temporal deep learning," *Sensors*, vol. 21, no. 6, pp. 2141, 2021.
[14] V. Ghate, "Hybrid deep learning approaches for smartphone sensor-based human activity recognition," *Multimedia Tool and Applications*, vol. 80, no. 28, pp. 35585–35604, 2021.
[15] I. D. Luptáková, M. Kubovčík and J. Pospíchal, "Wearable sensor-based human activity recognition with transformer model," *Sensors*, vol. 22, no. 5, pp. 1911, 2022.
[16] Z. Qin, Y. Zhang, S. Meng, Z. Qin and K. K. R. Choo, "Imaging and fusing time series for wearable sensor-based human activity recognition," *Information Fusion*, vol. 53, pp. 80–87, 2020.
[17] R. Mondal, D. Mukherjee, P. K. Singh, V. Bhateja and R. Sarkar, "A new framework for smartphone sensor-based human activity recognition using graph neural network," *IEEE Sensors Journal*, vol. 21, no. 10, pp. 11461–11468, 2020.
[18] M. Z. Uddin, M. M. Hassan, A. Alsanad and C. Savaglio, "A body sensor data fusion and deep recurrent neural network-based behavior recognition approach for robust healthcare," *Information Fusion*, vol. 55, pp. 105–115, 2020.
[19] J. Wu, L. Sun, D. Peng and S. Siuly, "A micro neural network for healthcare sensor data stream classification in sustainable and smart cities," *Computational Intelligence and Neuroscience*, vol. 2022, pp. 1–9, 2022.
[20] M. Alanazi, A. Alanazi, A. Almadhor and Z. A. Memon, "Multiobjective reconfiguration of unbalanced distribution networks using improved transient search optimization algorithm considering power quality and reliability metrics," *Scientific Reports*, vol. 12, no. 1, pp. 1–19, 2022.
[21] O. Banos, C. Villalonga, R. Garcia, A. Saez, M. Damas *et al.,* "Design, implementation and validation of a novel open framework for agile development of mobile health applications," *Biomedical Engineering*, vol. 14, no. 2, pp. S6, 2015.